ACS OMEGA

http://pubs.acs.org/journal/acsodf

Article

# Ultralong-Time Recovery and Low-Voltage Electroporation for Biological Cell Monitoring Enabled by a Microsized Multipulse Framework

Denise Lee, Sophia S. Y. Chan, Nemanja Aksic, Natasa Bajalovic,* and Desmond K. Loke*

Cite This: *ACS Omega* 2021, 6, 35325−35333

Read Online

ACCESS | Metrics & More | Article Recommendations | Supporting Information

**ABSTRACT:** Long-term nondestructive monitoring of cells is of significant importance for understanding cell proliferation, cell signaling, cell death, and other processes. However, traditional monitoring methods are limited to a certain range of testing conditions and may reduce cell viability. Here, we present a microgap, multishot electroporation (M2E) system for monitoring cell recovery for up to ∼2 h using ∼5 V pulses and with excellent cell viability using a medium cell population. Electric field simulations reveal the bias-voltage- and gap-size-dependent electric field intensities in the M2E system. In addition to excellent transparency with low cell toxicity, the M2E system does not require specialized components, expensive materials, complicated fabrication processes, or cell manipulations; it just consists of a micrometer-sized pattern and a low-voltage square-wave generator. Ultimately, the M2E system can offer a long-term and nontoxic method of cell monitoring.

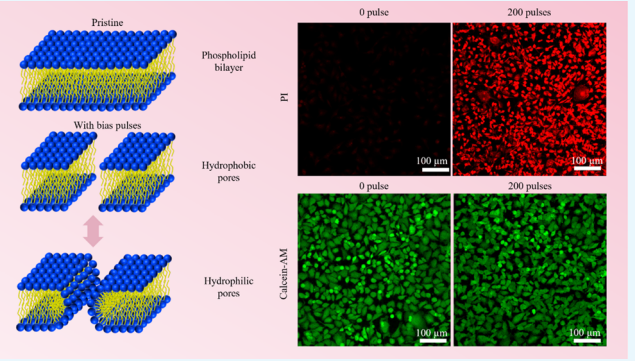


## 1. INTRODUCTION

Genetic and infectious diseases, including cancer and the novel coronavirus disease, have emerged as a serious global health concern. These diseases can cause millions of deaths and have a huge impact on global healthcare and socio-economic development.[1,2] A key challenge in fighting these diseases is the lack of effective drugs or specific treatments. Additionally, adverse side effects and increasing drug resistance owing to long-term use are serious issues. New and effective preventative and treatment strategies need to be developed urgently. Understanding cell behavior in various environments can lead to the design of these strategies. Investigations into cell behavior typically require understanding kinetics of the cell membrane permeabilization as a first step since the membrane is the primary barrier in cell-to-cell or cell-to-extracellular-matrix (ECM) interactions.[3] Moreover, understanding the mechanics behind membrane permeability may also improve current treatment strategies, minimize drug and reagent wastage, and increase the efficacy of these treatments.[4]

Chemical-based methods, such as molecular/fluorescent probes,[5−7] flow cytometry,[4,5] microfluidics devices, and other methods,[8−13] have been harnessed to understand membrane permeabilization. These techniques harness the size of cells and binding affinity of the cell membrane to various molecules for probing the cell behavior and offer excellent advantages such as high specificity, high cell-targeting accuracy, and high-resolution imaging at the single-cell level.[14,15] However, traditional methods tend to be serial and can have limited throughput for system biology analyses.[16]

Electrical-based monitoring approaches are promising candidates for understanding membrane permeabilization. Among other approaches, electroporation can be an elegant method for investigating membrane resealing in real time without chemical side effects.[17,18] Electroporation, based on administering electric fields to cells to increase the permeability of cell membranes, generally allows cells to be reused for subsequent analyses.[19−22] Additionally, impedance sampling does not require the use of additional reagents, which could potentially interfere with the membrane permeability during electroporation.[23] Moreover, electroporation can be utilized for a wide range of applications: (1) multianalyte delivery and detection systems, such as molecular probes,[24,25] fluorescence tags,[7,26−28] and cancer-targeting drugs,[29−31] (2) biological applications, such as the study of mutated membrane ion channels for neurobiological disorders,[32] investigating the evocation of neuro action potentials from the current source density measurements[33] and studying disease implantation

Received: August 9, 2021
Accepted: October 20, 2021
Published: December 13, 2021

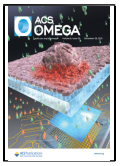

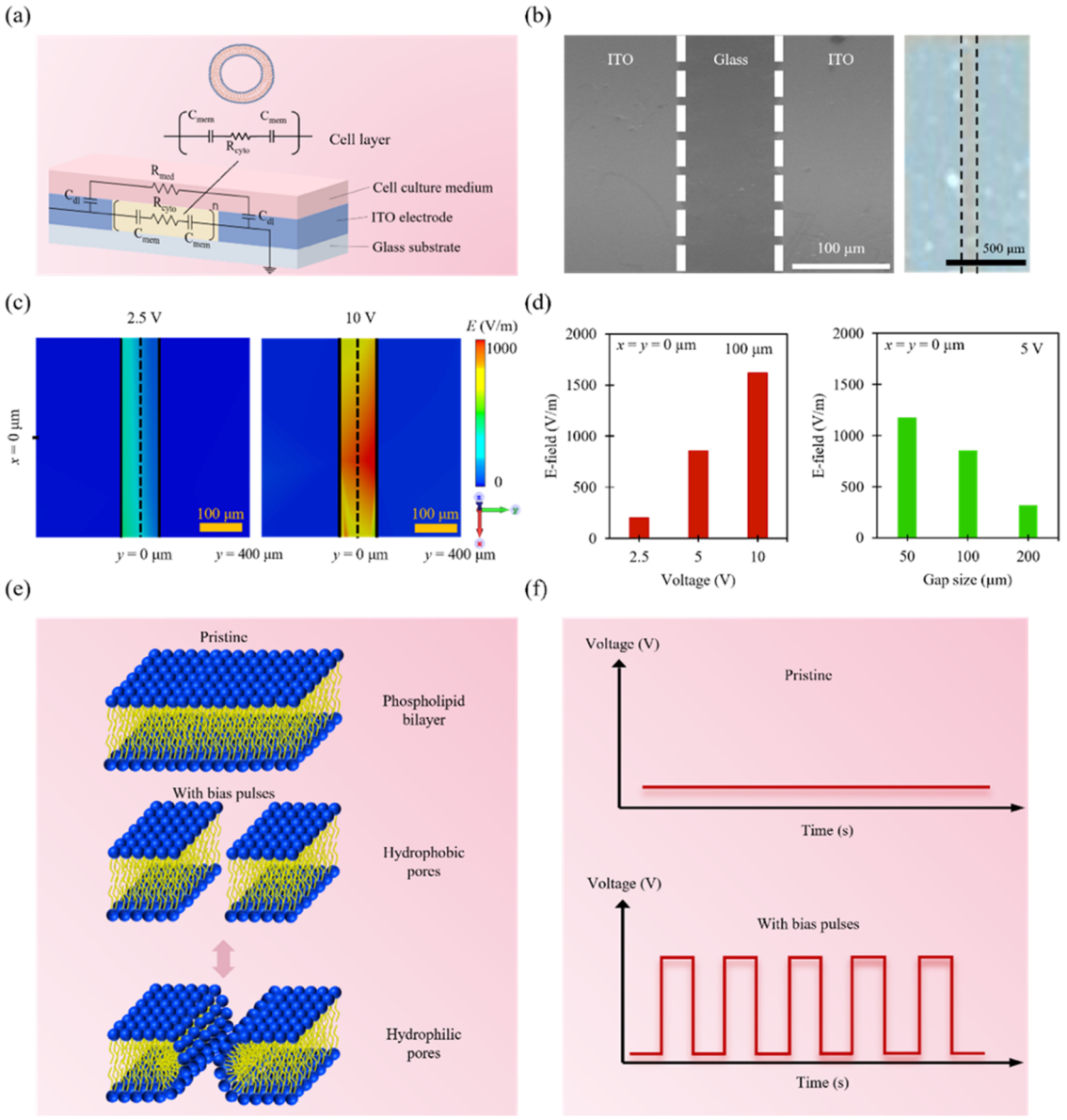


**Figure 1.** Overview of the experimental and computational framework of the M2E system. (a) Schematic illustration of the M2E system (bottom panel) and equivalent circuit model for the typical cell (top panel). (b) Scanning electron microscopy (SEM) image of the ITO subsystem with a gap size of ∼100 $\mu$m (left panel) and the actual photograph of the ITO subsystem (right panel). (c) Electric field distributions of an M2E system after applying ∼2.5 V (left panel) and ∼10 V (right panel) excitations. (d) Variations of electric field intensities in an M2E system with different bias voltage excitations (left panel) and gap sizes (right panel). (e) Schematic illustration of the process of pore formation in phospholipid bilayer after electroporation. (f) Schematic illustration of the voltage pulse waveforms.

models,[34,35] and (3) other applications including culture pacing and characterization studies,[36] wound healing studies[37−39] and other developmental biological studies. Besides, in electrochemotherapy applications, tumor cells can be permeabilized by electroporation, thereby enhancing their uptake of chemotherapeutic drugs, such as bleomycin and cisplatin.[40] Recently, single-cell electroporation and other types of devices have been explored for achieving low bias voltage electroporation devices.[41−44] Experiments have demonstrated a safe single-cell electroporation performed at small bias voltages.[45] However, the bias voltages used for generating strong electric fields for traditional electroporation tend to be large (tens of volts) as the distance between the electrodes utilized for conventional electroporation cuvettes/devices can be wide (millimeter length scale, see Supporting Information Table S3). Thus, our interest is in the use of a small bias voltage (below 10 V) for electroporation of medium cell population for substantially enhancing safety.

Electroporation involves the generation of pores in a cell membrane, where the resealing of pores plays a key role in preserving cell viability. Cell recovery processes, based on the resealing of the cell membrane, showing marked contrast in electrical impedance, are generally short on the 5−20 min timescale for 1−10 pulses.[46,47] Moreover, the time for cell recovery after electroporation has not yet been widely demonstrated and the definition of "cell recovery" can vary across studies. Some authors define cell recovery as a state in which impedance values are restored after a certain period of time, demonstrating that electroporated cells have recovered sufficiently to remain viable.[48,49] However, demonstration of


https://doi.org/10.1021/acsomega.1c04257
ACS Omega 2021, 6, 35325−35333

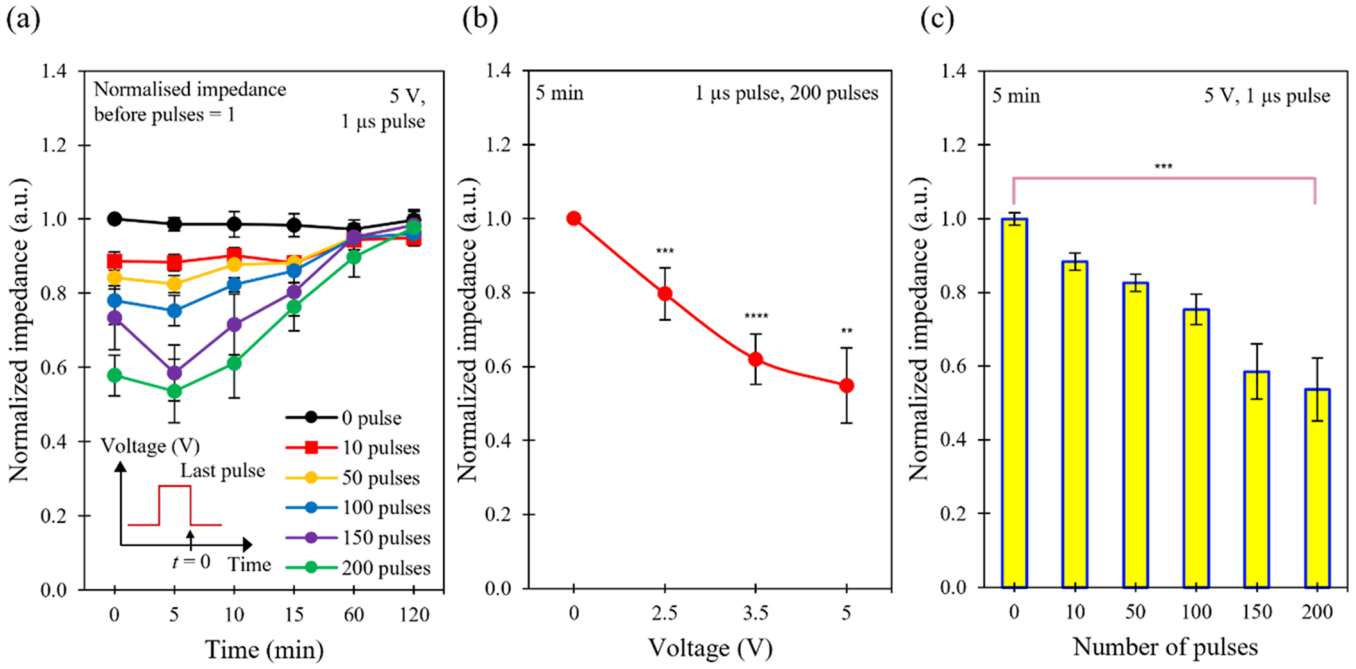


**Figure 2.** Electrical characteristics of the M2E system. (a) Time evolution of normalized impedance obtained for the system after electroporation with different number of pulses. The bias voltage was kept constant at ∼5 V and the pulse length was fixed at ∼1 μs. (b) Plot of normalized impedance as a function of bias voltage, measured ∼5 min after electroporation. The pulse length was kept constant at ∼1 μs and the number of pulses was fixed at 200 pulses. (c) Pulse-number-dependent normalized impedance values of the system. The bias voltage was kept constant at ∼5 V and the pulse length was fixed at ∼1 μs, measured ∼5 min after electroporation. Asterisks indicate the statistical significance of the difference in values between the control and test systems (** $p \leq 0.01$, *** $p \leq 0.001$, and **** $p \leq 0.0001$). Data are expressed as the standard error of mean (SEM) where $n = 6$.

cell recovery in the hour timescale, related to the enhancement of the time for pore-resealing processes, remains elusive. This can be important in the clinic, as it may lead to the optimization of treatment.

Here, we demonstrate a microgap multishot electroporation (M2E) system, building on a micrometer-sized (∼100 μm) and multipulse (0−200 pulses) framework for excellent monitoring of membrane permeability. The electric field simulations elucidate the bias-voltage- and gap-size-dependent electric field intensities in the M2E system. With the optimal number of pulses and voltage amplitude, the M2E system can capture cell processes in the MCF-7 cells with a recovery time of ∼2 h and using ∼5 V pulses while maintaining excellent cell viability using a medium cell population. Moreover, this would be the first demonstration of understanding membrane permeabilization using an electroporation system with a gap size of ∼100 μm for long-term monitoring of medium cell population in adherent cell lines (Supporting Information Table S3), which enables the use of low bias voltage pulses for enhancing safety. Additionally, in contrast with other conventional electroporation studies,[50,51] this work demonstrates the understanding of membrane permeabilization using an electroporation system without trypsinisation, which avoids altering cell responses for obtaining reliable information in the study of adherent cell lines. Furthermore, our investigation, in contrast to other traditional studies,[52−55] does not require specialized and complex equipment for system implementation and study.

## 2. RESULTS

A glass substrate was used as a starting material on which 650 nm thick indium−tin oxide (ITO) left and right electrodes were deposited for external circuit connection (Figure 1a). MCF-7 cells were then plated to complete the electroporation system, which we call the M2E system. The size of the gap between the left and right electrodes was chosen to be ∼100 μm (Figure 1b). To investigate the effects of electrical-bias conditions on cell permeabilization, the electric field distributions of the systems for different bias voltage excitations were simulated (Figure 1c). When the bias voltage administered to the system decreased (from 5 to 2.5 V), the intensity of the electric field decreased from 800 to 200 V/m (Figure 1d). In systems with different gap sizes, the intensities of the electric field can be modulated as well. A system with a gap size of ∼100 μm showed an electric field intensity of ∼800 V/m. Also, when the gap size of the system was decreased to ∼50 μm, the electric field intensity increased to ∼1100 V/m. As a result, low bias voltages (∼5 V) and small gap sizes (∼100 μm) can be achieved in the system, allowing the system to generate sufficiently strong electric fields for achieving excellent membrane permeabilization while maintaining good cell viability. Based on the simulation results, bias voltage pulses with various amplitudes (from 0 to 5 V) were administered to the cells. Different number of voltage pulses from 10 to 200 pulses were also utilized (Figure 1f). The impedance of the system was sampled at different times from 0 to 120 min. The electric field simulations reveal that a sufficiently large electric field can be achieved in the system at 5 V. Moreover, the upper bound of bias voltage provided by the testing system was 5 V. Based on these simulations and voltage bounds, for the experiments that involve different times after pulses and number of pulses, the bias voltage was chosen to be 5 V. The lower bound of the pulse length supplied by the testing system was 1 μs. Also, to achieve a short testing time


https://doi.org/10.1021/acsomega.1c04257
ACS Omega 2021, 6, 35325−35333

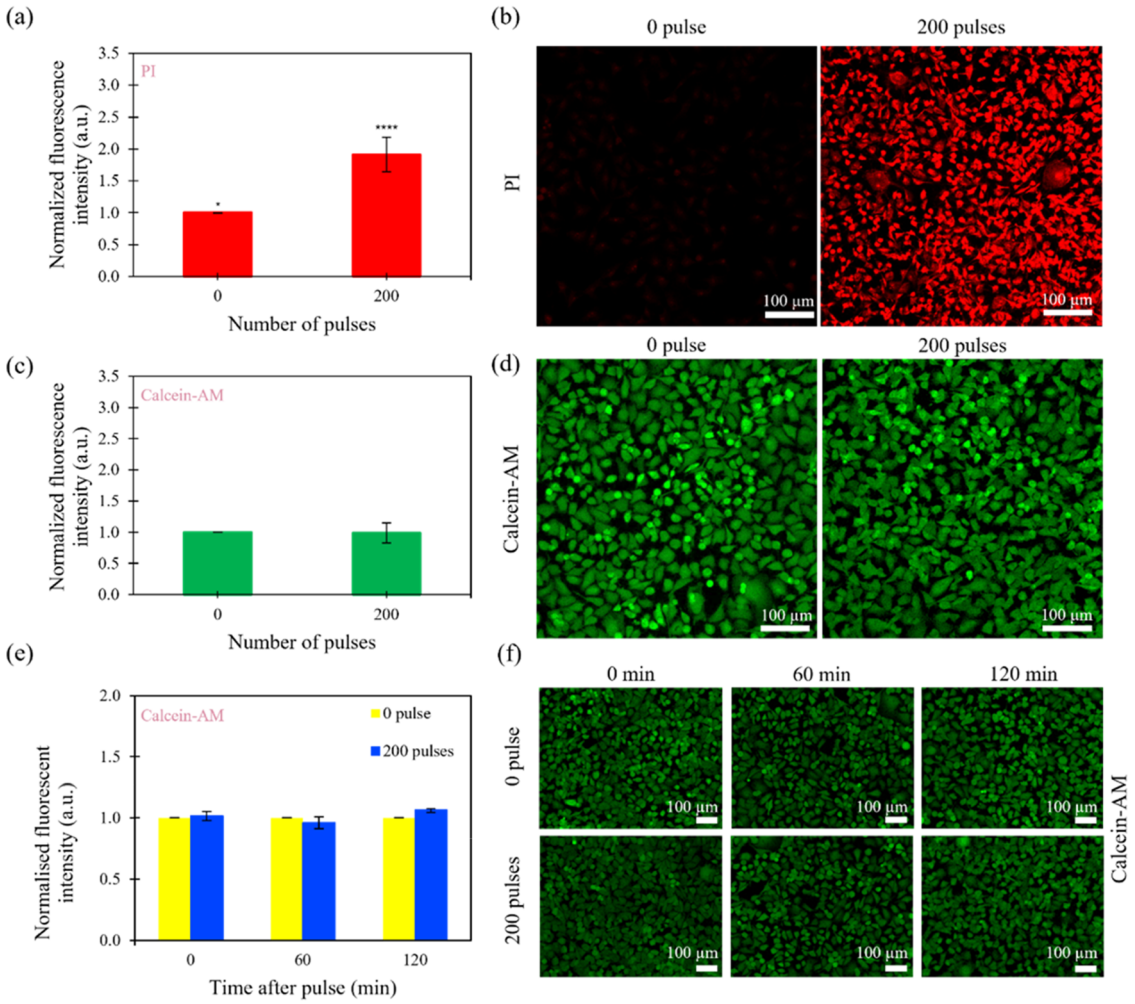


**Figure 3.** Pulse-number-dependent fluorescence intensity and cell viability of the cells after M2E electroporation. (a) Plot of the normalized fluorescence intensity as a function of the number of pulses and (b) fluorescence images of MCF-7 cells stained with PI after applying different number of pulses. (c) Plot of normalized fluorescence intensity as a function of the number of pulses and (d) fluorescence images of MCF-7 cells stained with calcein-AM after applying different number of pulses. (e) Plot of normalized fluorescence intensity as a function of time after applying 0 and 200 bias pulses and (f) fluorescent images of calcein-AM-stained MCF-7 cells sampled at different times after applying 0 and 200 bias pulses. The bias voltage and length of the pulses were kept constant at ∼5 V and ∼1 $\mu$s, respectively. Images were representative of other images taken in different fields of view using a microscope camera. Asterisks indicate the statistical significance between the control (0 pulse) and test systems (* $p \leq 0.05$ and **** $p \leq 0.0001$). Data are expressed as the standard error of the mean (SEM) for $n = 6$.

for the experiments that involve different times after pulses and number of pulses, the pulse length was selected to be 1 $\mu$s.

Complete cell recovery after electroporation generally comprises two processes. These processes may differ due to the types of pores created during electroporation: (1) partial recovery and (2) membrane resealing.[56−58] Most pores created in the process of partial recovery are temporary in nature, as the pores formed in a lipid bilayer of a membrane do not interact with other complex membrane organelles present in the membrane bilayer. These pores close rapidly and take place only a few minutes after electroporation.[59] Membrane resealing can occur at the same time. However, it is a slower process and includes the resealing of complex pores, such as metastable pores, that are formed due to the interaction of pores with various membrane proteins and cellular organelles. Metastable pores have a longer lifetime since the complexity of this pore structure makes it difficult for the cell membrane to undergo resealing.[46,47,60] These pores typically demonstrate a longer resealing time of 5−30 min after electroporation.[20,61]

This work demonstrates a cell recovery time of ∼2 h after electroporation of MCF-7 cells in the M2E system using the time between the onset of fall in the impedance values and return of the impedance values back to their original values as a measure of recovery time (Figure 2a, Supporting Information Table S2). This behavior can be due to the partial recovery and membrane resealing processes, where the transient pores and metastable pores are closed during this process. The recovery time observed here can exceed a baseline of ∼30 min for the state-of-the-art electroporation systems with medium cell populations (Supporting Information Table S3). This finding indicates that the partial recovery and membrane resealing processes can be described using our M2E system and might be used for obtaining a more complete picture of the membrane resealing process after electroporation of cells.

Generally, cell impedance can consist of two components: (1) cell membrane capacitance and (2) cell bulk resistance, which includes the resistance of other organelles and cytoplasm within the cell (Figure 1a).[62,63] During reversible electroporation, the capacitance of a cell membrane can


https://doi.org/10.1021/acsomega.1c04257
ACS Omega 2021, 6, 35325−35333

become negligible due to the creation of pores (Figure 1e), shorting the component of cell membrane impedance.[64] This can cause an immediate drop in cell impedance since the component of cell membrane capacitance disappears. As the cell membrane gradually reseals (Figure 1e), cell impedance can increase accordingly due to the restoration of the cell membrane capacitance. As a result, the electrical model provides the ability to correlate the pore formation and resealing with impedance sampling and to gain further insights into the dynamics of cell recovery using our M2E system.

With a low bias voltage, the electric field would be weak. As a result, we postulate that few and small-sized pores are induced on the cell membrane, with only a small drop in the impedance of the M2E system since most of the membrane barrier would still be preserved (Figure 2b, Supporting Information Table S4).[65,66] As the bias voltage increases, the electric field increases. Thus, the cell permeability would increase, resulting in a decrease in cell impedance. For example, the cells with 0 V show a normalized impedance value of 1.0, while the cells with 2.5 V show a lower normalized impedance value of ∼0.8 (normalized impedance = impedance of system at a target bias voltage/impedance of the system at 0 V). These findings agree well with the studies by other research groups.[20,67]

An increase in cell permeability can indicate a change in the number and type of pores that are generated. When higher electrical energy is delivered to the cells, for example, a higher number of pulses or bias voltage may allow for more pores to be formed.[68,69] Delivering higher electrical energy may also produce an increase in the proportion of transient pores compared to metastable pores in the pore population as well.[70,71] When subjected to an increasing number of pulses, the permeability of the cell membrane can increase (Figure 2c) since a higher number of pulses can indicate higher electric energy delivered to the cells. This suggests that a higher population of transient pores could be induced due to the increased energy delivered, thereby decreasing the measured impedance. The calculated energy delivered to the M2E system is ∼20 $\mu$J for a 10-pulse sequence ($E = n\frac{V^2}{R}t = 5 \times \frac{10^2}{50} \times 1 \times 10^{-6} = 10\,\mu\text{J}$, where $n$ is the number of pulses, $V$ is the bias voltage, $R$ is the resistance of the system, and $t$ is the length of the pulse). As a result, we were able to detect a corresponding decrease in system impedance with a higher number of pulses (Figure 2c). This was confirmed by our fluorescence experiments, where the cells stained with propidium iodide (PI) show an increase in fluorescence intensity with an increase in the number of bias voltage pulses (Figure 3a,b). Moreover, the cells electroporated by different number of pulses on the M2E system still remain viable, as shown by the relatively constant values of normalized fluorescence intensity when the cells were stained with calcein-AM (Figure 3c,d).

Several studies have speculated that subjecting cells to subsequent pulses with different delay times after the first pulse can reopen pores that have already resealed.[66,72] In conventional two-pulses protocols, the second pulse tends to produce a purely electrophoretically driven force to increase the intracellular concentrations (for the drug of choice). Demiryurek et al. have shown evidence to suggest that the second pulse additionally re-porate weakened cell membranes, which can explain the significant differences in transfection yield (Figure 3a) compared to single pulse electroporation protocols. Additionally, the pores generated from the weakened cell membranes can be nanosized, which can persist in the membrane for a long time. As such, it is possible that this theory could be extended to explain the response of a cell membrane to a train of pulses, where each pulse may cumulatively increase the number of nanosized pores (accumulation) and thus extend the recovery time of the cell membrane. This may explain why the cell recovery of our cells with multiple pulses (partial recovery and membrane resealing) in our M2E system, for bias voltage pulses ranging from 0 to 150 pulses, was ∼1 h, but when the number of pulses was increased to 200 pulses, a longer time of ∼2 h was observed. Additionally, the cells at different times after 0 and 200 bias voltage pulses also demonstrate excellent viability when the cells were stained with calcein-AM (Figure 3e,f). This indicates that using our M2E system, we can reseal the electroporated cell membranes completely, resulting in an intact cell membrane that allows the cells to undergo subsequent analytical processes without compromising their cellular integrity.

## 3. DISCUSSION

The main advantages of our system are as follows: (1) it allows us to observe the partial recovery and membrane resealing processes using impedance sampling for up to ∼2 h using ∼5 V pulses while maintaining excellent cell viability, proving to be a valuable method of determining the differences in cell response at different times after electroporation; (2) it is compact and portable such that cell sampling can be easily obtained; (3) it is easy to use, allowing various analysis tools to be implemented in conjunction; and (4) it is transparent, enabling excellent visual inspection of the cells and allowing the system to be used for fluorescence staining.

Another key advantage of our system is the ability to provide a label-free and real-time monitoring method. For example, with the use of microscale technologies, both electroporation and cellular assays could be integrated onto a single traditional electroporation system, allowing simultaneous electroporation and sampling of a single cell.[21] Although these systems may present a high level of integration, they can require a delicate level of operation as a slight change in pressure within the chamber can cause damage to the cell under study.[73] Moreover, a leakage pathway can occur if the pressure in the chamber is too low, hindering the electrical detection of pore formation. Currently, these systems depend on cell lysis labeling, and it is possible that they are unable to provide continuous snapshots of cellular behavior.[74] On the other hand, our system can provide a label-free and real-time method of obtaining cell responses. Furthermore, our system utilizes a medium population (approximately 6 000 to 10 000 cells), which can be necessary since most systems may have inherent heterogeneity within the population. This inherent heterogeneity may reduce the reliability of the observed results.[16,75]

A further advantage of our system can be that it allows both the growth and testing of cells using the same platform. In contrast, traditional methods may require different platforms for cell growth and testing.[76−78] For instance, our system allows the cells to be cultured, electroporated, and observed directly without the need for additional trypsinisation procedures. These procedures can cleave the cell membrane adhesion proteins[79] and affect both the complexity and morphology of cell membrane surfaces, which can inherently alter cell responses.[61,80] Furthermore, a series of cell analysis


https://doi.org/10.1021/acsomega.1c04257
ACS Omega 2021, 6, 35325−35333

steps can be performed for the cell population under test without compromising the quality of the information obtained.

A limitation to achieving real-time cell monitoring is the small size of the system. The volume of the cell media that the system can hold is limited, which presents a level of complexity when designing an experiment. Although regular media replenishments can be performed, the system may limit the maximum number of cells plated to 8000 when the experiments require the cells to be alive for more than two hours. Additionally, larger cell populations may not allow us to accurately quantify cell viability since minor changes in cell fluorescence may not be detectable using an overconfluent cell population. As a result, the cell population needs to be carefully considered before using the system for these experiments.

Another aspect that can limit the real-time cell monitoring of the system is the limited evaluation of cell recovery mechanisms. Traditional methods for real-time monitoring can be limited by the viability of the cell line after electroporation. Moreover, the number of studies that can be performed on the same cell population is limited. Further work on the recovery mechanism may be achieved by the appropriate combination of the programming schemes and device structures for optimizing system performance.

Another limitation of the system can be the nonuniformity of the electric field distribution in a cell membrane. In our simulation, the cancerous cell membrane is significantly less electrically conductive (∼5.30 μS/m) compared to the intracellular (∼130 mS/m) and extracellular (∼600 mS/m) media.[81] Without a pulsed electric field, pore formation is absent, and the bias electric field across the membrane is nonexistent. After a pulsed electric field is applied, a nonuniform distribution of electric field across the membrane can be formed, which may be dependent on the positions of the cathode and anode.[81] The presence of different electric field regions within the cell reveals that the peak electric field in the cell interior is smaller compared to the extracellular region when a pulsed electric field is applied (Supporting Information Figure S2).

As the strength of the electric field increases, the distribution of the electric field across the membrane can become more nonuniform. Moreover, the asymmetry in bias voltage distribution and differences in membrane conductivity and permeability, pore density, and pore size in both the plasma and intracellular membrane regions may influence the distribution of the electric field across the membrane.[82] Generally, modeling bulk electroporation processes can result in the formation of the peak electric field only at the cell membrane, which gradually decays away from the membrane region.[83]

A lack of uniformity in the distribution of electric field in a cell membrane may result in a disruption in the ion-transport-controlled process, an unequal spatial opening of generated pores, and early apoptosis.[83] To minimize these side effects, the optimization of electric field parameters such as the bias voltage amplitude, the length of pulses, the strength of the electric field, and the frequency of bias voltage pulses is necessary. Moreover, there is a need for further studies related to how the nonisotropic conductivity of the structures may improve the uniformity of the distribution of the electric field across the membrane.

## 4. CONCLUSIONS

In this current work, we demonstrated that M2E can enable ultralong-time recovery and low-voltage electroporation for monitoring the membrane permeability of cancer cells. Electric field simulations disclose the bias-voltage- and gap-size-dependent electric field intensities in the M2E system. Unlike other traditional monitoring methods that can require specialized monitoring components, expensive materials, a complicated fabrication process, and multiple cell manipulation, M2E is based on a micrometer-sized pattern and a low-voltage pulse generator which are generally accessible to standard laboratories. It is possible that with its excellent transparency and ease of use, M2E can offer a long-time recovery, low-voltage method for cell process monitoring.

## 5. METHODS

**5.1. System Fabrication.** The custom-built microgap, multishot electroporation (M2E) system consists of the ITO subsystem and MCF-7 cells (Figure 1a). The 650 nm thick left and right indium−tin oxide (ITO) electrodes were sputtered on top of a glass substrate. The width of the gap between the electrodes was chosen to be ∼100 μm. MCF-7 cells were plated to complete the electroporation system. Scanning electron microscopy (SEM) images of the system are shown in Figure 1b. Cell chambers (Sigma) were attached to the ITO subsystem for cell storage.

**5.2. Cell Culture.** MCF-7 cells were cultured in phenol-red-containing Dulbecco's modified Eagle's medium (DMEM) (Nacalai Tesque), supplemented with 7.5% fetal bovine serum (FBS) (Sigma) and 2 mM L-glutamine (Gibco). Cells were incubated at 37 °C in a humidified atmosphere of 5% $CO_2$.

**5.3. Experimental Setup.** The ITO subsystems were sterilized in 70% ethanol for 20 min and then exposed to ultraviolet (UV) irradiation for another 20 min. The MCF-7 cells were plated on each ITO subsystem at a density of $8 \times 10^3$ cells per well and incubated for 24 h prior to an experiment.

**5.4. Electrical Setup and Protocol for Electroporation.** Prior to impedance sampling, the cells were washed with 120 μL of Dulbecco's phosphate-buffered saline (DPBS) (Gibco) and 120 μL of fresh Dulbecco's modified Eagle's medium (DMEM) was added. Cells were electroporated with bias voltage pulses of different amplitudes from 0 to 5 V and different number of pulses from 0 to 200 pulses.

An arbitrary-waveform generator (Tektronix) was used to program different number of pulses or bias voltages, which was delivered to the cells via external circuitry, and the signals at different times after passing through the cells were analyzed with an oscilloscope (Tektronix). The schematic of the pulse sequence used can be seen in Figure 1f. The testing setup is illustrated in the Supporting Figure S1. $R_{cell}$ represents cell impedance, which can be calculated by eqs 1 and 2

$$I = \frac{V_{out}}{R_3} \tag{1}$$

$$R_{cell} = \frac{V_{in} - V_{out}}{I} - R_2 \tag{2}$$

After electroporation, cell impedance was then calculated for different times from 0 to 120 min. Thereafter, normalized cell impedance was calculated (normalized impedance = impe-



https://doi.org/10.1021/acsomega.1c04257
ACS Omega 2021, 6, 35325−35333

dance of system with the target number of pulses/impedance of system with 0 pulse).

**5.5. Fluorescence Intensity Analysis.** To monitor and assess the degree of electroporation, two types of fluorescence dyes were used to demonstrate the efficiency of electroporation and cell viability. For fluorescence intensity analysis, the cells were washed with 120 $\mu$L of DPBS and the media were replaced with 120 $\mu$L of fresh DMEM containing 0.03 mM propidium iodide (PI) (Thermo Fisher) and/or 0.1 $\mu$M of calcein-AM (Sigma Aldrich) before electroporation. After electroporation, the cells were left to rest before fixation with 2% formaldehyde (Sigma Aldrich) and imaged using a fluorescence microscope. Images were taken at 10 different fields of the sample, among which six were chosen and processed with ImageJ. The fluorescence intensity values were then obtained from each image and normalized against control samples, i.e., the cells that experienced no pulse.

**5.6. Simulation Procedure.** To investigate the electric field distribution of the M2E system, a finite-element simulation of the model was conducted using commercial software (CST Microwave Studio and ANSYS). The system was modeled with an assumed homogeneous cell layer to simplify the simulation calculations. In a frequency-domain solver, Maxwell's equations were transformed into the frequency domain while assuming that the fields and excitation sources were time-harmonic-dependent. The solver can be described by the following equation:

$$E = R\{\underline{E}(\omega)\exp(j\omega t)\} \quad (3)$$

The parameters used in the simulation are shown in the Supporting Table S1. The electric field distributions of the model with different bias voltages were calculated.

## ■ ASSOCIATED CONTENT

### Supporting Information

The Supporting Information is available free of charge at https://pubs.acs.org/doi/10.1021/acsomega.1c04257.

Schematic illustration of electrical setup; simulations of electric field distributions of four cells; table of parameters used for simulation model; comparison of electroporation systems; and raw impedance values of the experiments used in this study (PDF)

## ■ AUTHOR INFORMATION


### Corresponding Authors

**Natasa Bajalovic** − *Department of Science, Mathematics and Technology, Singapore University of Technology and Design, Singapore 487372, Singapore*; Email: natasa_bajalovic@sutd.edu.sg

**Desmond K. Loke** − *Department of Science, Mathematics and Technology, Singapore University of Technology and Design, Singapore 487372, Singapore; Office of Innovation, Changi General Hospital, Singapore 529889, Singapore*; orcid.org/0000-0001-5799-6441; Email: desmond_loke@sutd.edu.sg

### Authors

**Denise Lee** − *Department of Science, Mathematics and Technology, Singapore University of Technology and Design, Singapore 487372, Singapore*

**Sophia S. Y. Chan** − *Department of Science, Mathematics and Technology, Singapore University of Technology and Design, Singapore 487372, Singapore*; orcid.org/0000-0001-6710-0469

**Nemanja Aksic** − *Department of Science, Mathematics and Technology, Singapore University of Technology and Design, Singapore 487372, Singapore*

Complete contact information is available at: https://pubs.acs.org/10.1021/acsomega.1c04257


### Notes

The authors declare no competing financial interest.

## ■ ACKNOWLEDGMENTS

We thank J. S. Naikar, W. C. Teoh, and L. T. Ng for inspiring discussions. This work was supported by the Ministry of Education, Singapore (MOE2017-T2-2-064), MIT-SUTD International Design Centre, Changi General Hospital-SUTD, Singapore (CGH-SUTD-HTIF2019-001), SUTD-Zhejiang-University (SUTD-ZJU (VP) 201903), and National Supercomputing Centre, Singapore (15001618) grant programs. D. Lee, S. S.-Y. Chan, and N. Aksic thank the Ministry of Education and SUTD for the scholarship support.

## ■ REFERENCES


(1) Baldwin, R.; Weder, B.; Mauro, D. *Economics in the Time of COVID-19*; CEPR Press, 2020.

(2) Richards, M.; Anderson, M.; Carter, P.; Ebert, B. L.; Mossialos, E. The Impact of the COVID-19 Pandemic on Cancer Care. *Nat. Cancer* **2020**, *1*, 565−567.

(3) Weaver, J. C. Electroporation of Biological Membranes from Multicellular to Nano Scales. *IEEE Trans. Dielectr. Electr. Insul.* **2003**, *10*, 754−768.

(4) Canatella, P. J.; Karr, J. F.; Petros, J. A.; Prausnitz, M. R. Quantitative Study of Electroporation-Mediated Molecular Uptake and Cell Viability. *Biophys. J.* **2001**, *80*, 755−764.

(5) Soueid, M.; Dobbelaar, M. C. F.; Bentouati, S.; Bardet, S. M.; O'Connor, R. P.; Bessières, D.; Paillol, J.; Leveque, P.; Arnaud-Cormos, D. Delivery Devices for Exposure of Biological Cells to Nanosecond Pulsed Electric Fields. *Med. Biol. Eng. Comput.* **2018**, *56*, 85−97.

(6) Williams, S. J.; Prescher, J. A. Building Biological Flashlights: Orthogonal Luciferases and Luciferins for in Vivo Imaging. *Acc. Chem. Res.* **2019**, 3039.

(7) Tian, M.; Ma, Y.; Lin, W. Fluorescent Probes for the Visualization of Cell Viability. *Acc. Chem. Res.* **2019**, *52*, 2147−2157.

(8) Wang, K.; Zhao, Y.; Chen, D.; Fan, B.; Lu, Y.; Chen, L.; Long, R.; Wang, J.; Chen, J. Specific Membrane Capacitance, Cytoplasm Conductivity and Instantaneous Young's Modulus of Single Tumour Cells. *Sci. Data* **2017**, *4*, No. 170015.

(9) Zheng, G.; Patolsky, F.; Cui, Y.; Wang, W. U.; Lieber, C. M. Multiplexed Electrical Detection of Cancer Markers with Nanowire Sensor Arrays. *Nat. Biotechnol.* **2005**, *23*, 1294−1301.

(10) Ye, N.; Qin, J.; Shi, W.; Liu, X.; Lin, B. Cell-Based High Content Screening Using an Integrated Microfluidic Device. *Lab Chip* **2007**, *7*, 1696−1704.

(11) Song, H.; Chen, T.; Zhang, B.; Ma, Y.; Wang, Z. An Integrated Microfluidic Cell Array for Apoptosis and Proliferation Analysis Induction of Breast Cancer Cells. *Biomicrofluidics* **2010**, *4*, No. 044104.

(12) Ma, Q.; Wang, J.; Li, Z.; Lv, X.; Liang, L.; Yuan, Q. Recent Progress in Time-Resolved Biosensing and Bioimaging Based on Lanthanide-Doped Nanoparticles. *Small* **2019**, *15*, No. 1804969.

(13) Zhao, Q.; Huang, C.; Li, F. Phosphorescent Heavy-Metal Complexes for Bioimaging. *Chem. Soc. Rev.* **2011**, *40*, 2508−2524.

(14) Wang, J. Electrochemical Biosensors: Towards Point-of-Care Cancer Diagnostics. *Biosens. Bioelectron.* **2006**, *21*, 1887−1892.

(15) Stoeva, S. I.; Lee, J. S.; Smith, J. E.; Rosen, S. T.; Mirkin, C. A. Multiplexed Detection of Protein Cancer Markers with Biobarcoded Nanoparticle Probes. *J. Am. Chem. Soc.* **2006**, *128*, 8378−8379.
(16) Halldorsson, S.; Lucumi, E.; Gómez-Sjöberg, R.; Fleming, R. M. T. Advantages and Challenges of Microfluidic Cell Culture in Polydimethylsiloxane Devices. *Biosens. Bioelectron.* **2015**, *63*, 218−231.
(17) Chen, Y.; Moser, M. A. J.; Luo, Y.; Zhang, W.; Zhang, B. Chemical Enhancement of Irreversible Electroporation: A Review and Future Suggestions. *Technol. Cancer Res. Treat.* **2019**, *18*, No. 1533033819874128.
(18) Xiong, Z.; Yao, C.; Zhou, W.; Liu, Y.; Li, C. Low Voltage Irreversible Electroporation Induced Apoptosis in HeLa Cells. *J. Cancer Res. Ther.* **2012**, *8*, 80.
(19) Hug, T. S. Biophysical Methods for Monitoring Cell-Substrate Interactions in Drug Discovery. *Assay Drug Dev. Technol.* **2003**, *1*, 479−488.
(20) Guo, X.; Zhu, R. Controllable In-Situ Cell Electroporation with Cell Positioning and Impedance Monitoring Using Micro Electrode Array. *Sci. Rep.* **2016**, *6*, No. 31392.
(21) Lee, W. G.; Demirci, U.; Khademhosseini, A. Microscale Electroporation: Challenges and Perspectives for Clinical Applications. *Integr. Biol.* **2009**, *1*, 242−251.
(22) Krukiewicz, K. Electrochemical Impedance Spectroscopy as a Versatile Tool for the Characterization of Neural Tissue: A Mini Review. *Electrochem. Commun.* **2020**, *116*, No. 106742.
(23) Dermol, J.; Pakhomova, O. N.; Pakhomov, A. G.; Miklavčič, D. Cell Electrosensitization Exists Only in Certain Electroporation Buffers. *PLoS One* **2016**, *11*, No. e0159434.
(24) Ceppi, L.; Bardhan, N. M.; Na, Y.; Siegel, A.; Rajan, N.; Fruscio, R.; Del Carmen, M. G.; Belcher, A. M.; Birrer, M. J. Real-Time Single-Walled Carbon Nanotube-Based Fluorescence Imaging Improves Survival after Debulking Surgery in an Ovarian Cancer Model. *ACS Nano* **2019**, *13*, 5356−5365.
(25) Qian, Y.; Karpus, J.; Kabil, O.; Zhang, S. Y.; Zhu, H. L.; Banerjee, R.; Zhao, J.; He, C. Selective Fluorescent Probes for Live-Cell Monitoring of Sulphide. *Nat. Commun.* **2011**, *2*, No. 495.
(26) Zhao, Q.; Huang, H.; Li, F. Phosphorescent Heavy-Metal Complexes for Bioimaging. *Chem. Soc. Rev.* **2011**, *40*, 2508−2524.
(27) Oudeng, G.; Au, M.; Shi, J.; Wen, C.; Yang, M. One-Step in Situ Detection of MiRNA-21 Expression in Single Cancer Cells Based on Biofunctionalized MoS2 Nanosheets. *ACS Appl. Mater. Interfaces* **2018**, *10*, 350−360.
(28) Liu, L.; Lv, R. J.; Leung, J. K.; Zou, Q.; Wang, Y.; Li, F.; Liang, W.; Feng, S.; Wu, M. Y. A Near-Infrared Biothiol-Specific Fluorescent Probe for Cancer Cell Recognition. *Analyst* **2019**, *144*, 4750−4756.
(29) Padma, V. V. An Overview of Targeted Cancer Therapy. *BioMedicine* **2015**, *5*, 1−6.
(30) Rembiałkowska, N.; Dubińska-Magiera, M.; Sikora, A.; Szlasa, W.; Szewczyk, A.; Czapor-Irzabek, H.; Daczewska, M.; Saczko, J.; Kulbacka, J. Doxorubicin Assisted by Microsecond Electroporation Promotes Irreparable Morphological Alternations in Sensitive and Resistant Human Breast Adenocarcinoma Cells. *Appl. Sci.* **2020**, *10*, No. 2765.
(31) Dong, X.; Yin, W.; Zhang, X.; Zhu, S.; He, X.; Yu, J.; Xie, J.; Guo, Z.; Yan, L.; Liu, X.; Wang, Q.; Gu, Z.; Zhao, Y. Intelligent MoS2 Nanotheranostic for Targeted and Enzyme-/PH-/NIR-Responsive Drug Delivery to Overcome Cancer Chemotherapy Resistance Guided by PET Imaging. *ACS Appl. Mater. Interfaces* **2018**, *10*, 4271−4284.
(32) Terrettaz, S.; Vogel, H. Investigating the Function of Ion Channels in Tethered Lipid Membranes by Impedance Spectroscopy. *MRS Bull.* **2005**, *30*, 207−210.
(33) Pettersen, K. H.; Devor, A.; Ulbert, I.; Dale, A. M.; Einevoll, G. T. Current-Source Density Estimation Based on Inversion of Electrostatic Forward Solution: Effects of Finite Extent of Neuronal Activity and Conductivity Discontinuities. *J. Neurosci. Methods* **2006**, *154*, 116−133.
(34) Ativanichayaphong, T.; Tang, S. J.; Hsu, L. C.; Huang, W. D.; Seo, Y. S.; Tibbals, H. F.; Spechler, S.; Chiao, J. C. *An Implantable Batteryless Wireless Impedance Sensor for Gastroesophageal Reflux Diagnosis*, 2010 IEEE MTT-S International Microwave Symposium, 2010; pp 608−611.
(35) Hartmann, C. J.; Wojtecki, L.; Vesper, J.; Volkmann, J.; Groiss, S. J.; Schnitzler, A.; Südmeyer, M. Long-Term Evaluation of Impedance Levels and Clinical Development in Subthalamic Deep Brain Stimulation for Parkinson's Disease. *Parkinsonism Relat. Disord.* **2015**, *21*, 1247−1250.
(36) Diemert, S.; Dolga, A. M.; Tobaben, S.; Grohm, J.; Pfeifer, S.; Oexler, E.; Culmsee, C. Impedance Measurement for Real Time Detection of Neuronal Cell Death. *J. Neurosci. Methods* **2012**, *203*, 69−77.
(37) Cai, W.; Ni, D.; Long, Y.; Wang, X.; Yao, G.; Gibson, A. L.; Lan, X.; Li, J.; Wei, H.; Jiang, Y.; Yu, B. Effective Wound Healing Enabled by Discrete Alternative Electric Fields from Wearable Nanogenerators. *ACS Nano* **2018**, *12*, 12533−12540.
(38) Davenport, N. R.; Sonnemann, K. J.; Eliceiri, K. W.; Bement, W. M. Membrane Dynamics during Cellular Wound Repair. *Mol. Biol. Cell* **2016**, *27*, 2272−2285.
(39) Thakral, G.; LaFontaine, J.; Najafi, B.; Talal, T. K.; Kim, P.; Lavery, L. A. Electrical Stimulation to Accelerate Wound Healing. *Diabetic Foot Ankle* **2013**, No. 22081.
(40) Gehl, J. Electroporation: Theory and Methods, Perspectives for Drug Delivery, Gene Therapy and Research. *Acta Physiol. Scand.* **2003**, *177*, 437−447.
(41) Huang, Y.; Rubinsky, B. Micro-Electroporation: Improving the Efficiency and Understanding of Electrical Permeabilization of Cells. *Biomed. Microdevices* **1999**, *2*, 145−150.
(42) Lundqvist, J. A.; Sahlin, F.; Åberg, M. A. I.; Strömberg, A.; Eriksson, P. S.; Orwar, O. Altering the Biochemical State of Individual Cultured Cells and Organelles with Ultramicroelectrodes. *Proc. Natl. Acad. Sci. USA* **1998**, *95*, 10356−10360.
(43) Teissie, J.; Tsong, T. Y. Electric Field Induced Transient Pores in Phospholipid Bilayer Vesicles. *Biochemistry* **1981**, *20*, 1548−1554.
(44) Wang, M.; Orwar, O.; Olofsson, J.; Weber, S. G. Single-Cell Electroporation. *Anal. Bioanal. Chem.* **2010**, *397*, 3235−3248.
(45) Dong, Z.; Jiao, Y.; Xie, B.; Hao, Y.; Wang, P.; Liu, Y.; Shi, J.; Chitrakar, C.; Black, S.; Wang, Y. C.; Lee, L. J.; Li, M.; Fan, Y.; Chang, L. On-Chip Multiplexed Single-Cell Patterning and Controllable Intracellular Delivery. *Microsyst. Nanoeng.* **2020**, *6*, 2.
(46) Lopez, A.; Rols, M. P.; Teissie, J. 31p NMR Analysis of Membrane Phospholipid Organization In Viable, Reversibly Electropermeabilized Chinese Hamster Ovary Cells. *Biochemistry* **1988**, *27*, 1222−1228.
(47) Neumann, E.; Toensing, K.; Kakorin, S.; Budde, P.; Frey, J. Mechanism of Electroporative Dye Uptake by Mouse B Cells. *Biophys. J.* **1998**, *74*, 98−108.
(48) Zhang, Z.; Zheng, T.; Zhu, R. Single-Cell Individualized Electroporation with Real-Time Impedance Monitoring Using a Microelectrode Array Chip. *Microsyst. Nanoeng.* **2020**, *6*, No. 81.
(49) Stolwijk, J. A.; Hartmann, C.; Balani, P.; Albermann, S.; Keese, C. R.; Giaever, I.; Wegener, J. Impedance Analysis of Adherent Cells after in Situ Electroporation: Non-Invasive Monitoring during Intracellular Manipulations. *Biosens. Bioelectron.* **2011**, *26*, 4720−4727.
(50) Hyder, I.; Eghbalsaied, S.; Kues, W. A. Systematic Optimization of Square-Wave Electroporation Conditions for Bovine Primary Fibroblasts. *BMC Mol. Cell Biol.* **2020**, *21*, No. 9.
(51) Yao, S.; Rana, S.; Liu, D.; Wise, G. E. Electroporation Optimization to Deliver Plasmid DNA into Dental Follicle Cells. *Biotechnol. J.* **2009**, *4*, 1488−1496.
(52) Chang, D. C. Cell Poration and Cell Fusion Using an Oscillating Electric Field. *Biophys. J.* **1989**, *56*, 641−652.
(53) Kinosita, K.; Tsong, T. Y. Voltage-Induced Conductance in Human Erythrocyte Membranes. *Biochim. Biophys. Acta, Biomembr.* **1979**, *554*, 479−497.


https://doi.org/10.1021/acsomega.1c04257
*ACS Omega* 2021, 6, 35325−35333

(54) Teruel, M. N.; Meyer, T. Electroporation-Induced Formation of Individual Calcium Entry Sites in the Cell Body and Processes of Adherent Cells. *Biophys. J.* **1997**, *73*, 1785−1796.
(55) Marszalek, P. E.; Farrell, B.; Verdugo, P.; Fernandez, J. M. Kinetics of Release of Serotonin from Isolated Secretory Granules. I. Amperometric Detection of Serotonin from Electroporated Granules. *Biophys. J.* **1997**, *73*, 1160−1168.
(56) Saulis, G.; Venslauskas, M. S.; Naktinis, J. Kinetics of Pore Resealing in Cell Membranes after Electroporation. *J. Electroanal. Chem. Interfacial Electrochem.* **1991**, *321*, 1−13.
(57) Kandušer, M.; Šentjurc, M.; Miklavčič, D. Cell Membrane Fluidity Related to Electroporation and Resealing. *Eur. Biophys. J.* **2006**, *35*, 196−204.
(58) Saulis, G. Pore Disappearance in a Cell after Electroporation: Theoretical Simulation and Comparison with Experiments. *Biophys. J.* **1997**, *73*, 1299−1309.
(59) Choi, Y.-S.; Kim, H.-B.; Kim, S.-H.; Choi, J.; Park, J.-K. Microdevice for Analyzing the Effect of Electrochemotherapy on Cancer Cells. *Anal. Chem.* **2009**, *81*, 3517−3522.
(60) Kotnik, T.; Rems, L.; Tarek, M.; Miklavčič, D. Membrane Electroporation and Electropermeabilization: Mechanisms and Models. *Annu. Rev. Biophys.* **2019**, *48*, 63−91.
(61) García-Sánchez, T.; Sánchez-Ortiz, B.; Vila, I.; Guitart, M.; Rosell, J.; Gómez-Foix, A. M.; Bragós, R. Design and Implementation of a Microelectrode Assembly for Use on Noncontact in Situ Electroporation of Adherent Cells. *J. Membr. Biol.* **2012**, *245*, 617−624.
(62) Ma, Z.; Liu, J.; Shentu, X.; Bian, Y.; Yu, X. Optimization of Electroporation Conditions for Toyocamycin Producer Streptomyces Diastatochromogenes 1628. *J. Basic Microbiol.* **2014**, *54*, 278−284.
(63) Deng, J.; Schoenbach, K. H.; Buescher, E. S.; Hair, P. S.; Fox, P. M.; Beebe, S. J. The Effects of Intense Submicrosecond Electrical Pulses on Cells. *Biophys. J.* **2003**, *84*, 2709−2714.
(64) Sundararajan, R. *Electroporation-Based Therapies for Cancer: From Basics to Clinical Applications*; Woodhead Publishing, 2014.
(65) Yao, C.; Lv, Y.; Zhao, Y.; Dong, S.; Liu, H.; Ma, J. Synergistic Combinations of Short High-Voltage Pulses and Long Low-Voltage Pulses Enhance Irreversible Electroporation Efficacy. *Sci. Rep.* **2017**, *7*, No. 15123.
(66) Demiryurek, Y.; Nickaeen, M.; Zheng, M.; Yu, M.; Zahn, J. D.; Shreiber, D. I.; Lin, H.; Shan, J. W. Transport, Resealing, and Re-Poration Dynamics of Two-Pulse Electroporation-Mediated Molecular Delivery. *Biochim. Biophys. Acta, Biomembr.* **2015**, *1848*, 1706−1714.
(67) Sweeney, D. C.; Weaver, J. C.; Davalos, R. V. Characterization of Cell Membrane Permeability In Vitro Part I: Transport Behavior Induced by Single-Pulse Electric Fields. *Technol. Cancer Res. Treat.* **2018**, *17*, No. 1533033818792491.
(68) Aslam, M. A.; Riaz, K.; Mahmood, M. Q.; Zubair, M. Hybrid Analytical-Numerical Approach for Investigation of Differential Effects in Normal and Cancer Cells under Electroporation. *RSC Adv.* **2019**, *9*, No. 41518.
(69) Krassowska, W.; Filev, P. D. Modeling Electroporation in a Single Cell. *Biophys. J.* **2007**, *92*, 404−417.
(70) Pavlin, M.; Miklavčič, D. Theoretical and Experimental Analysis of Conductivity, Ion Diffusion and Molecular Transport during Cell Electroporation - Relation between Short-Lived and Long-Lived Pores. *Bioelectrochemistry* **2008**, *74*, 38−46.
(71) Leguèbe, M.; Silve, A.; Mir, L. M.; Poignard, C. Conducting and Permeable States of Cell Membrane Submitted to High Voltage Pulses: Mathematical and Numerical Studies Validated by the Experiments. *J. Theor. Biol.* **2014**, *360*, 83−94.
(72) Rems, L.; Miklavčič, D. Tutorial: Electroporation of Cells in Complex Materials and Tissue. *J. Appl. Phys.* **2016**, *119*, No. 201101.
(73) Le Gac, S.; van Uitert, I. Electroporation in Microfluidic Devices. In *Handbook of Electroporation*; Springer, 2016; pp 1−20.
(74) Nan, L.; Jiang, Z.; Wei, X. Emerging Microfluidic Devices for Cell Lysis: A Review. *Lab Chip* **2014**, *14*, 1060−1073.
(75) Yuan, G. C.; Cai, L.; Elowitz, M.; Enver, T.; Fan, G.; Guo, G.; Irizarry, R.; Kharchenko, P.; Kim, J.; Orkin, S.; Quackenbush, J.; Saadatpour, A.; Schroeder, T.; Shivdasani, R.; Tirosh, I. Challenges and Emerging Directions in Single-Cell Analysis. *Genome Biol.* **2017**, *18*, No. 84.
(76) Chan, S. S.; Tan, Y. S.; Wu, K.-X.; Cheung, C.; Loke, D. K. Ultra-High Signal Detection of Human Embryonic Stem Cells Driven by Two-Dimensional Materials. *ACS Appl. Bio Mater.* **2018**, *1*, 210−215.
(77) Potter, H.; Heller, R. Transfection by Electroporation. *Curr. Protoc. Mol. Biol.* **2003**, *9*, 9-3.
(78) Kurosawa, O.; Oana, H.; Matsuoka, S.; Noma, A.; Kotera, H.; Washizu, M. Electroporation through a Micro-Fabricated Orifice and Its Application to the Measurement of Cell Response to External Stimuli. *Meas. Sci. Technol.* **2006**, *17*, 3127.
(79) Huang, H. L.; Hsing, H. W.; Lai, T. C.; Chen, Y. W.; Lee, T. R.; Chan, H. T.; Lyu, P. C.; Wu, C. L.; Lu, Y. C.; Lin, S. T.; Lin, C. W.; Lai, C. H.; Chang, H. T.; Chou, H. C.; Chan, H. L. Trypsin-Induced Proteome Alteration during Cell Subculture in Mammalian Cells. *J. Biomed. Sci.* **2010**, *17*, No. 36.
(80) Wegener, J.; Keese, C. R.; Giaever, I. Recovery of Adherent Cells after in Situ Electroporation Monitored Electrically. *Biotechniques* **2002**, *33*, 348−357.
(81) Kotnik, T.; Kramar, P.; Pucihar, G.; Miklavčič, D.; Tarek, S. M. Cell Membrane Electroporation— Part 1: The Phenomenon. *IEEE Electr. Insul. Mag.* **2012**, *28*, 14−23.
(82) Frey, W.; White, J. A.; Price, R. O.; Blackmore, P. F.; Joshi, R. P.; Nuccitelli, R.; Beebe, S. J.; Schoenbach, K. H.; Kolb, J. F. Plasma Membrane Voltage Changes during Nanosecond Pulsed Electric Field Exposure. *Biophys. J.* **2006**, *90*, 3608−3615.
(83) Mukherjee, P.; Nathamgari, S. S. P.; Kessler, J. A.; Espinosa, H. D. Combined Numerical and Experimental Investigation of Localized Electroporation-Based Cell Transfection and Sampling. *ACS Nano* **2018**, *12*, 12118−12128.


https://doi.org/10.1021/acsomega.1c04257
*ACS Omega* 2021, 6, 35325−35333